Stress wave mitigation at suture interfaces

2017 Biomed. Phys. Eng. Express 3 035025

(http://iopscience.iop.org/2057-1976/3/3/035025)

IOP Publishing Biomed. Phys. Eng. Express 3 (2017) 035025 https://doi.org/10.1088/2057-1976/aa777e

Biomedical Physics & Engineering Express

CrossMark

RECEIVED
7 March 2017

ACCEPTED FOR PUBLICATION
6 June 2017

PUBLISHED
23 June 2017

PAPER

Stress wave mitigation at suture interfaces

Nayeon Lee[1,2], Lakiesha N Williams[1,2], Sungkwang Mun[1], Hongjoo Rhee[1,3], R Prabhu[1,2], Kabindra R Bhattarai[4] and M F Horstemeyer[1,3]

[1] Center for Advanced Vehicular Systems, Mississippi State University, Mississippi State, MS 39762-5405, United States of America
[2] Department of Agricultural and Biological Engineering, Mississippi State University, Mississippi State, MS 39762-9632, United States of America
[3] Department of Mechanical Engineering, Mississippi State University, Mississippi State, MS 39762-9552, United States of America
[4] Department of Mechanical Engineering, Florida State University, Tallahassee, FL 32310-6046, United States of America

E-mail: nayeon@cavs.msstate.edu

Keywords: suture, sinusoidal interface, stress mitigation, stress wave, wave scattering, damping

Abstract

This study investigated the stress wave dissipation in sinusoidal patterned suture interfaces that were inspired by sutures in biological materials. Finite element results showed that a sutured interface decreased the pressure 37% more than that at an unsutured interface, which arose from wave scattering and greater energy dissipation at sinusoidal boundaries. Stress wave scattering resulted in converting compressive waves (S11) into orthogonal flexural (S22) and shear waves (S12), which decreased both the peak pressure (attenuation) and wave speed (dispersion). Higher strain energy occurring at sutured interfaces brought energy loss within viscoelastic gap, too. In addition, we parameterized several variables related to the suture interfaces for their influence in stress wave mitigation. The following seven parameters were examined: (1) waviness of suture (ratio of suture height to suture period), (2) ratio of the suture height over the entire bar thickness, (3) gap thickness, (4) elastic modulus, (5) type of the boundary, (6) impact amplitude, and (7) impact duration. The final result of the parametric study revealed that the high ratio of the suture over the entire bar thickness had the greatest influence, followed by the short impact duration, and then by the low elastic modulus. Additionally, a high ratio of the suture over the entire bar thickness and low elastic modulus decreased the stress wave velocity as well. These findings can be applied for designing various synthetic damping systems so that manmade engineering designs can implement the optimized sutures for impact scenarios.

1. Introduction

Biological materials are remarkably designed for efficient mechanical behavior. One elegant example is a suture joint, which is a simple geometry yet multifunctional. In biological structures, suture joints are commonly found where two stiff components interlock each other. For example, within the microstructure of the woodpecker beak, a wavy sinusoidal-geometry was observed under the transmission electron microscope (figure 1(a)). Compared to other birds, whose beaks' impact resistance is less than that of woodpeckers, the waviness of suture shown in woodpeckers' beaks is greater (Lee *et al* 2014). Figure 1(b) shows bison's cranial suture, which has been extensively researched. Researchers reported that cranial sutures provide flexibility for growth, movement and strain due to masticatory and impact energy dissipation (Hubbard *et al* 1971, Behrents *et al* 1978, Jaslow 1990, Herring and Teng 2000, Opperman 2000, Sun *et al* 2004, Yu *et al* 2004, Byron 2006, Seimetz *et al* 2012, Curtis *et al* 2013). As shown in figure 1(c), the ammonoid fossil also shows a wavy structure with a hierarchical fractal pattern on its shell. The suture of the ammonoid fossil has been studied to investigate its mechanical role and relation between hierarchical structures of sutures and function (Allen 2006, 2007, Ubukata *et al* 2010). De Blasio (2008) reported that complex suture lines dramatically diminished the strain and the stress in the phragmocone such that suture fluted septum reinforced the shell against hydrostatic pressure. The turtle shell also has suture joints in their carapace as shown in figure 1(d). Krauss *et al* (2009) conducted three-point bending tests on the suture-contained turtle bony shell and reported that the turtle shell withstands small loads by low-stiffness

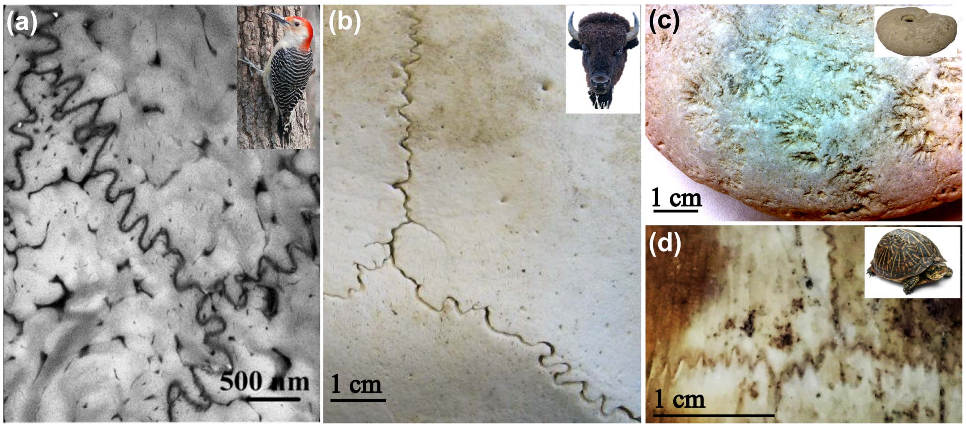

Figure 1. Suture lines in biological materials; (a) suture line shown at the tip of woodpecker beaks (keratin); (b) cranial suture in a bison skull (bone); (c) wavy line in a surface of an ammonoid fossil (calcium carbonate), and; (d) suture at a box turtle (bone).

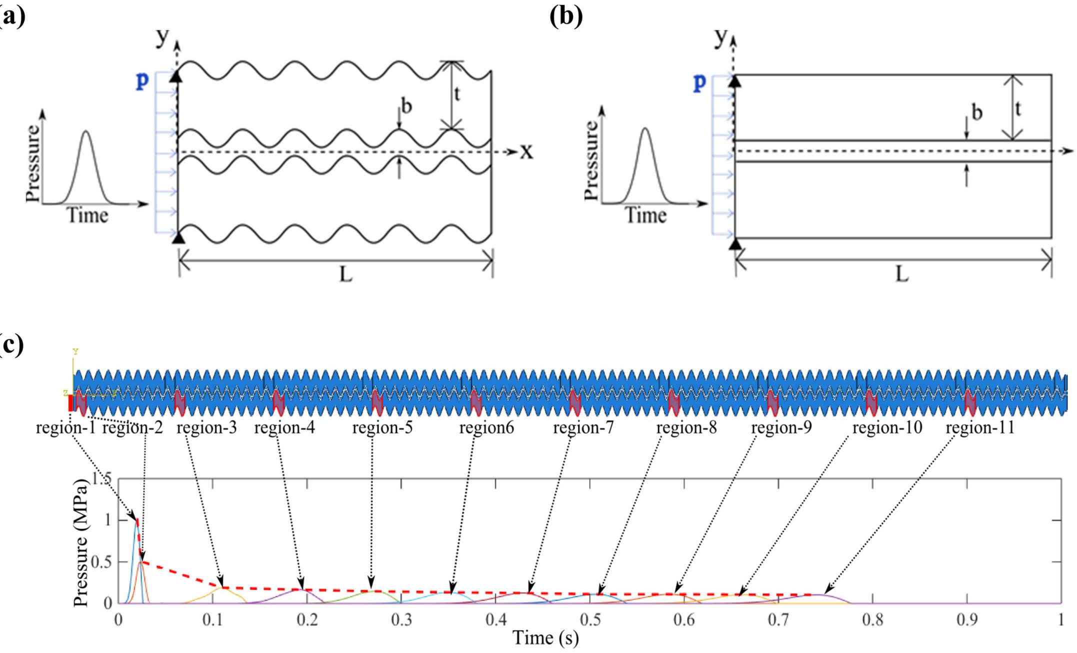

Figure 2. (a) Idealized two-dimensional bar with a suture interface of gap thickness of b. The dimension of the bar is $L = 1000$ mm, $t = 15$ mm, and $b = 2$ mm. The pressure initiated on the left side of the bar. (b) Schematic of an idealized bar with a flat interface. (c) Following an initial impact pressure applied in Region 1, the pressure data were recorded at the eleven regions indicated by the red regions in the bar. Then, the peak pressures were connected by the red dotted line in the graph. As the pressure wave propagated in the bar, the peak pressure decreased.

deformation and becomes much stiffer when the external load increases beyond a certain threshold. The suture of the leatherback turtle was also studied and revealed that the suture caused the balance between tension and shear, and brought structural flexibility by causing angular displacement (Chen *et al* 2015).

Mechanically, the wavy suture can greatly enhance the strength of materials. Jaslow (1990) experimentally studied mechanical properties of sutures and reported that the suture increased bending strength. Similar results on the tensile strength and bending strength have been reported as the suture plays a key role as an additive to increase strength (Li *et al* 2011, 2012b, 2013, 2014a, 2014b). In addition, a study of an interfacial crack with hierarchical sinusoidal sutures found that sutures enhance interfacial fracture toughness under Mode-I and Mode-II loadings (Li *et al* 2012a).

Although sutures are often found in the spot that dynamic responses occur, mechanisms of aforementioned properties of sutures during impact loading have not been extensively studied. Jaslow (1990)

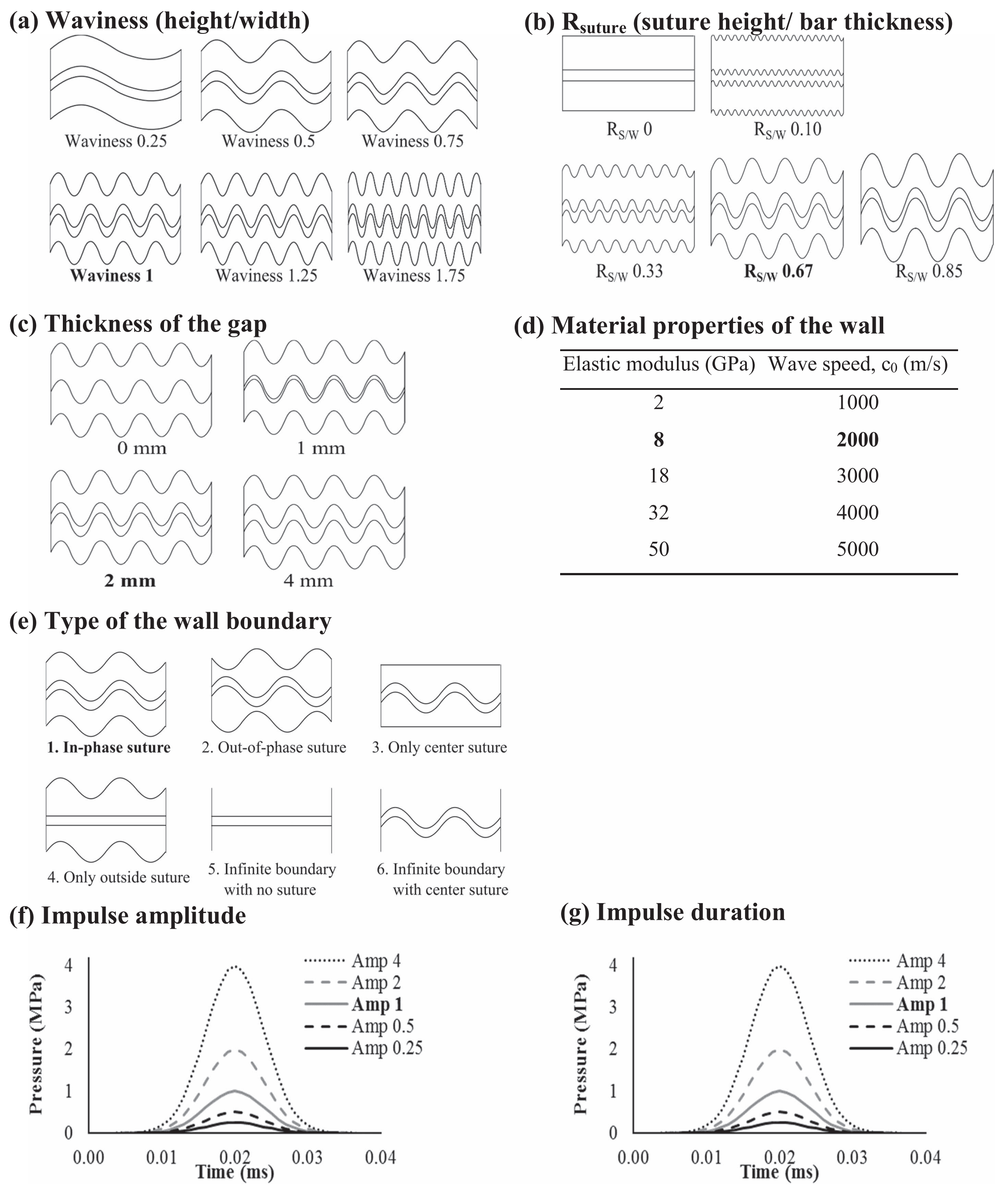

Figure 3. Seven variables influencing the stress wave mitigation; (1) suture waviness (ratio of suture height to suture period), (2) R_{suture}, the ratio of the suture height to the bar thickness, (3) thickness of the gap, (4) material properties of the elastic wall, (5) type of boundary, (6) Amplitude of the impact, and (7) impact duration. The default values are in bold font.

studied energy absorption using a pendulum on the cranial sutures of head-butting goats. Using finite element (FE) analysis, the role of cranial sutures was investigated by Maloul *et al* (2014), who quantified how sutures redistributed the stress. Zhang and Yang (2015) pointed out that hierarchically designed cranial sutures benefited the stress attenuation and energy absorption.

The main objective of the present study is to investigate the geometrical effects of sinusoidal sutures on the stress wave mitigation by using FE models. The following sections detail the simulation setup, results, discussion, and conclusions.

2. Simulation set up

An idealized bar with a sutured interface (i.e., sutured bar) and an idealized bar with a flat interface (i.e., unsutured bar) were created and analyzed from two-dimensional FE analysis in Abaqus/Explicit under dynamic conditions. As shown in figures 2(a) and (b), the dimension of the bar was 32 mm $\times$ 1000 mm, in which one side of the bar was 15 mm $\times$ 1000 mm with a gap thickness of 2 mm. The wall was treated as an elastic and isotropic material with Young's modulus $E = 8$ GPa, Poisson's ratio $\nu = 0.3$, and density $\rho = 2000$ kg m^{-3}, and those material properties generated a longitudinal wave speed of 2000 m s^{-1}. The impact load was a Gaussian impulse and applied on the left side of the bar as shown in figures 2(a) and (b) with the end nodes, on the same side, fully constrained to the y-direction. The sutured and unsutured gaps were treated as a viscoelastic material in which the hyperelastic Ogden model was employed with the elastic parameters, μ and a, being 15.6 KPa and 21.4 (Cheng and Gan 2007), respectively. The viscoelastic properties were assigned by a Prony series with the viscoelastic parameters, d and t, being 0.549 and 6.01 s, respectively, which were determined from a rat muscle study (Bosboom *et al* 2001). For meshing, a plane stress 4-noded element (CPS4R) was used, and the approximate element size was 0.5 mm generating about 100 000 number of elements in the 2D bars. Then, a parametric study was performed to understand the dependence of suture geometric variables and the external impact load. The seven variables were; (1) suture waviness, (2) R_{suture} (ratio of the suture height to the entire bar thickness), (3) suture gap thickness, (4) elastic modulus of the wall, (5) geometry of the bar boundary walls, (6) amplitude of external impact load, and (7) impact duration. The detail of the experimental case is described in figure 3. While examining one variable, the other variables were fixed.

In order to measure the extent of dissipation in the sutured bar, pressure–time history data were recorded at eleven regions along the bar at every 100 mm, indicated by red regions in figure 2(c). The damping capability of the sutured bar was then evaluated through the damping quotient, which is the ratio of the pressure decay from the 'Region-1' compared to 'Region-11' as the following:

$$\text{Damping quotient} = \frac{\text{Pressure}_{\text{region-1}} - \text{Pressure}_{\text{region-11}}}{\text{Pressure}_{\text{region-1}}}. \quad (1)$$

Further, the normalized phase velocity was also analyzed to investigate the influence of sutures on wave dispersion. The following is the equation for the normalized velocity

$$\text{Normalized velocity} = \frac{\text{Phase velocity at current bar}}{\text{Phase velocity at unsutured bar}}. \quad (2)$$

3. Results and discussion

FE simulations were carried out by applying external mechanical loads to produce a stress wave that propagated in a continuum media. We examined the damping capability of suture interfaces by comparing to an unsutured interface bar. Then, the variables of the suture interfaces such as the geometric variations and boundary conditions were assessed by their influence on the stress wave mitigation (pressure reduction of the traveling wave within the bar).

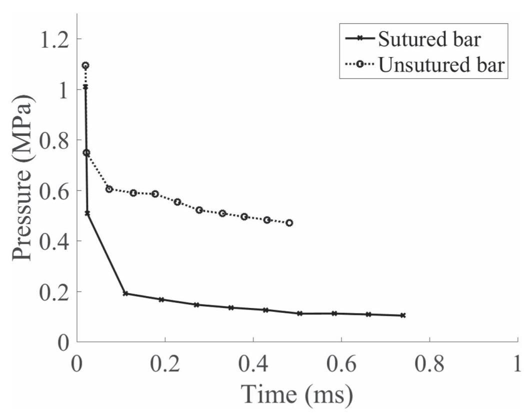

Figure 4. Comparison of pressure recorded along the sutured bar and unsutured bar. Each point represents the peak pressure at the eleven regions. The initial impact was 1 MPa, and the pressure when stress waves reached to the end was 0.47 MPa for the unsutured bar and 0.1 MPa for the sutured bar.

3.1. Dissipation of stress waves in the suture interface

A sutured interface was able to reduce the stress wave effectively compared to an unsutured interface. Figure 4 shows the peak pressure decay in the sutured compared to an unsutured bar. The initial load was 1 MPa, and the peak pressure when the stress wave reached the end of the bar was 0.47 MPa for the unsutured bar and 0.1 MPa at the sutured bar. While 53% of the initial pressure dissipated during the pressure wave traveled the unsutured bar, 90% of the initial pressure dissipated at the sutured bar. The sutured bar pressure was 37% less than that of the unsutured bar over the bar length used in this study.

There were two mechanisms associated with the sutured bar for stress wave mitigation as compared to the unsutured bar. First, stress wave scattering occurred at the boundary of the sutured bar, in which compressive waves (S11) were converted into shear waves (S12) and into orthogonal flexural waves (S22). From a wave perspective, there are two basic types of wave motion for mechanical waves: longitudinal waves and shear waves (also called transverse waves). Displacements in longitudinal waves occur in a parallel direction to the wave propagation, and in transverse waves, displacements occur in a perpendicular direction (Graff 1975). The waves related to S11 and S22 are longitudinal waves, and the waves related to S12 are shear waves.

Wave scattering is an interaction of waves with a boundary or obstacles in a medium resulting in wave reflection, transmission, or refraction (Brekhovskikh and Goncharov 2012). Since the compressive incidence impinged the sinusoidal interfaces, wave scattering can be considered a reflection at a curved surface as described in figure 5. The reflected waves consist of longitudinal and shear waves with angles of θ_L and θs, respectively. According to DasGupta and Hagedorn (2007), wave scattering at boundaries can be

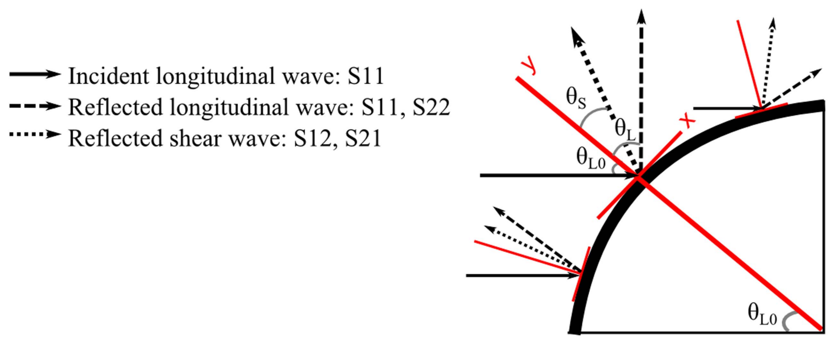

Figure 5. Reflections of compressive incidence waves striking a curved boundary. The incident longitudinal wave with an angle of θ_{L0} reflected to a longitudinal wave with an angle of θ_L and a shear wave with an angle of θ_S.

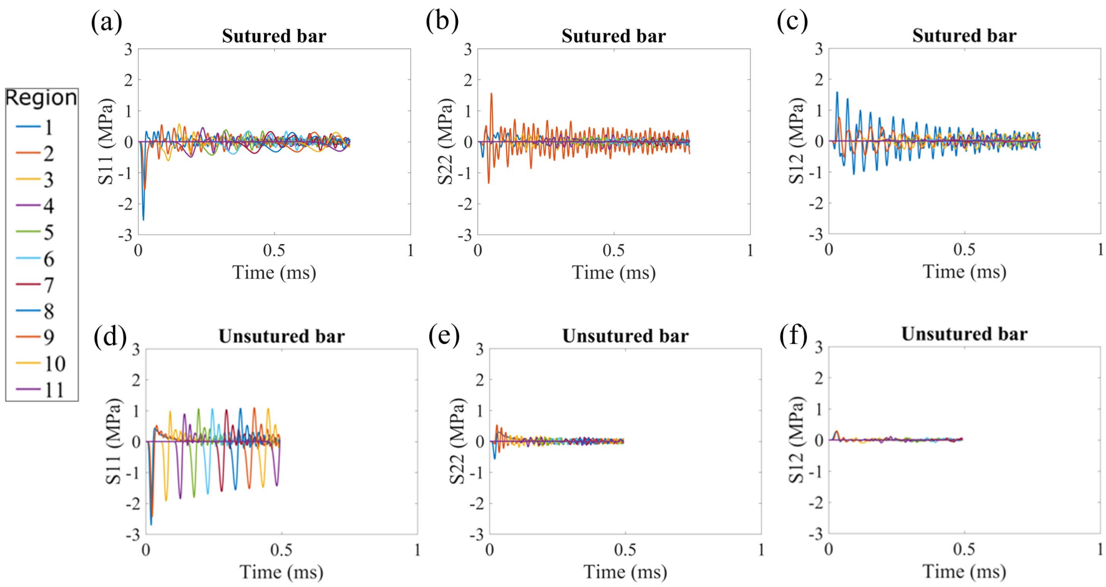

Figure 6. Stress waves shown as a function of time in the eleven regions along the sutured bar illustrating the stress components of (a) S11, (b) S22, (c) S12, and along the unsutured bar also illustrating (d) S11, (e) S22, and (f) S12. The stress waves were plotted until the wave reached the end of the bar. For the sutured bar, the stress wave reached the end at 0.78 ms, and for the unsutured bar, the stress wave reach the end at 0. 55 ms.

defined as the following numerical expression. The total wave field can be represented as the following:

$$u(x,\,y,\,t) = A_{L0}\hat{n}_{L0}\mathrm{e}^{\mathrm{i}\kappa_{L0}\{x\,\sin\theta_{L0}+y\,\cos\theta_{L0}-C_L t\}} + A_L\hat{n}_L\mathrm{e}^{\mathrm{i}\kappa_L\{x\,\sin\theta_L-y\,\cos\theta_L-C_L t\}} + A_S\hat{a}\times\hat{n}_S\mathrm{e}^{\mathrm{i}k_S\{x\,\sin\theta_S-y\,\cos\theta_S-C_S t\}}, \tag{3}$$

where u is the displacement, t is the time, A is the amplitude, κ is the wave number, and θ is the angle between the waves. $L0$, L, and S are the incident waves, reflected longitudinal waves, and reflected shear waves, respectively. The directions of the waves are

$$\hat{n}_{L0} = (\sin\theta_L,\ \cos\theta_L)^T,\quad \hat{n}_L = (\sin\theta_L,\ -\cos\theta_L)^T,\quad \hat{n}_S = (\sin\theta_S,\ -\cos\theta_S)^T. \tag{4}$$

Also, the speeds of longitudinal wave and shear wave are

$$C_L = \sqrt{\frac{E}{\rho}}, \tag{5}$$

$$C_S = \sqrt{\frac{E}{2\rho(1+\gamma)}}, \tag{6}$$

where E is Young's modulus, γ is the Poisson ratio, and ρ is the density. For given material properties in this study, $C_L = 2000$ m s^{-1} and $C_S = 1240.3$ m s^{-1}. With an assumption that a reflecting surface is a free surface, then the boundary conditions are as follows:

$$\sigma_{12}|_{y=0} = 0,\quad \sigma_{22}|_{y=0} = 0. \tag{7}$$

The boundary conditions produce the following relationships:

$$\kappa_{L0}\sin\theta_{L0} = \kappa_L\sin\theta_L = \kappa_S\sin\theta_S,\quad C_L\kappa_{L0} = C_L\kappa_L = C_S\kappa_s. \tag{8}$$

Then,

$$\theta_L = \theta_{L0},\quad \theta_S = \frac{C_S}{C_L}\theta_{L0}. \tag{9}$$

For the given conditions of this study, the angles of the reflected longitudinal waves are the same as the

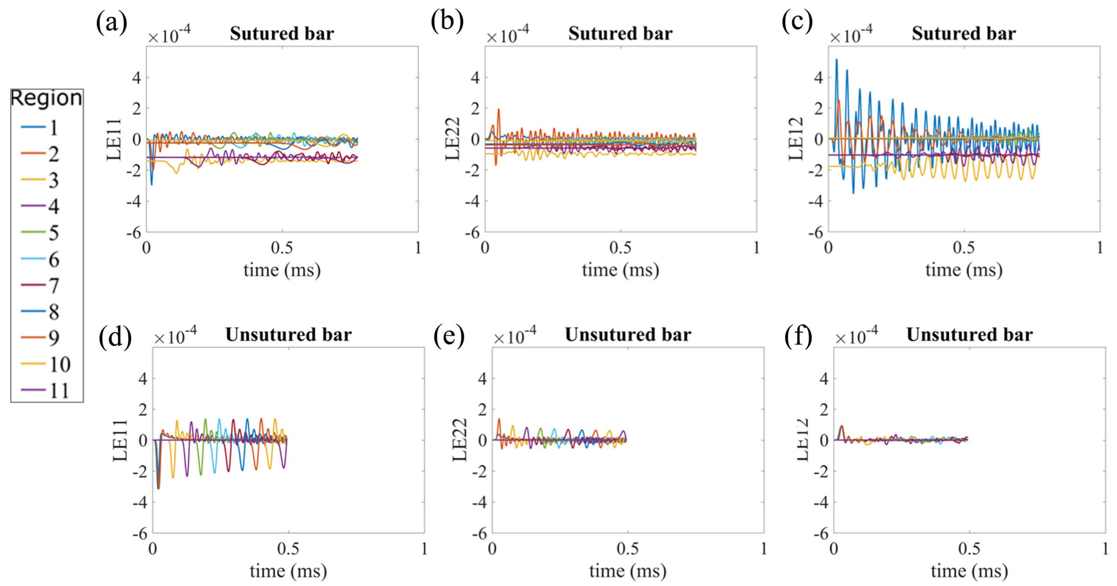

Figure 7. Strain in the eleven regions along the sutured bar for the strain components of (a) LE11, (b) LE22, (c) LE12 and along the unsutured bar for the stress components of (d) LE11, (e) LE22, and (f) LE12.

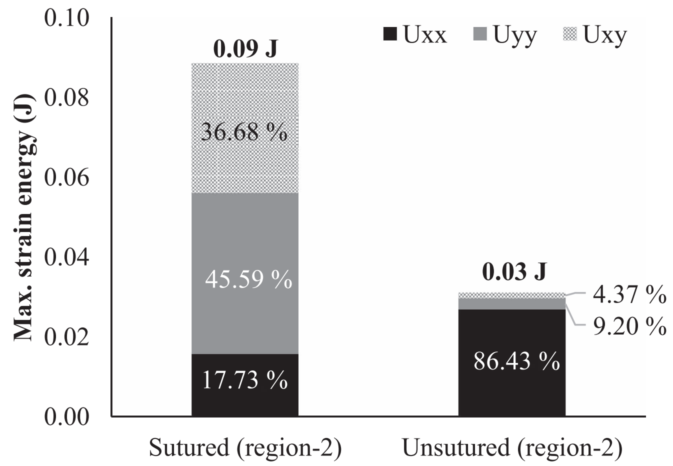

Figure 8. Maximum strain energy density associated with different displacements in the x, y, and z directions for the sutured and unsutured bar in Region 2 (indicated in figure 2(c)) near the initial impact location. The total strain energy is greater for the sutured bar than that of the unsutured bar because the strain energy to yy and xy direction is much greater at the sutured bar.

angles of incident longitudinal waves. On the other hand, the angles of reflected shear waves are 0.53 times the angles of the incident longitudinal waves.

As a result of wave scattering at the suture interfaces, the magnitude of S11 decreased, and S12 and S22 increased (figure 6). The maximum S22 generated in the sutured bar was 1.58 MPa approximately three times greater than that of the unsutured bar with S22 equaling 0.54 MPa; the maximum S12 generated in the sutured bar was 1.59 MPa approximately five times greater than that of the unsutured bar with S12 equaling 0.29 MPa. Not only does one observe a pressure decay but also wave dispersion from wave scattering. The wave speed determined from equation (5) is 2000 m s^{-1} when there are no boundary effects. In the unsutured bar with boundaries, the wave speed decreased to 1818.18 m s^{-1} and arrived at 0.55 ms. Alternatively, in the sutured bar with boundaries, the wave speed decreased to 1282.05 m s^{-1} and arrived at the free end at 0.78 ms. Accordingly, the sutured bar induced y-direction longitudinal (LE22) and shear strains (LE12). Figure 7 shows that the sutured bar induced strains in the y-direction and shear direction but decreased strains in the x-direction.

Figure 8 shows the maximum strain energy density in the sutured and unsutured bar at Region-2 (near-front region) where the sinusoidal suture began so that the wave scattering started early. The peak strain energy was 0.09 J in the sutured bar and 0.03 J in the unsutured bar. Hence, the sutured bar incurred approximately three times greater strain energy than that of unsutured bar. Specifically, in the sutured bar,

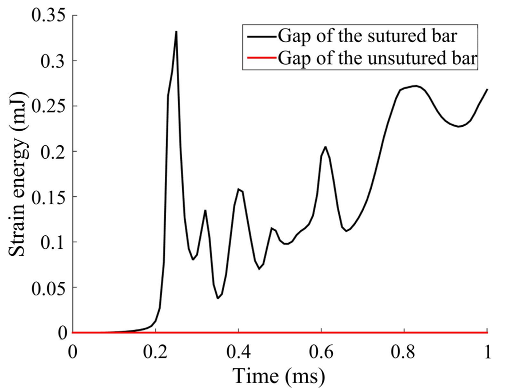

Figure 9. Strain energy occurring at the gap of the sutured bar (black) compared to the unsutured bar (red).

the strain energy was stored in all directions of *xx* (17.73%), *yy* (45.59), and *xy* (36.68%) due to reflected stress waves, while in the unsutured bar most of the strain energy stored was only in the *xx* direction (86.43%).

Another mechanism that reduced the amplitude of the traveling pressure wave was related to the strain energy being stored in the viscoelastic suture gap. It is common to interleave viscoelastic layers between hard and stiff material to increase the damping of the structure (Saravanos and Pereira 1992, Cupiał and Nizioł 1995, Berthelot *et al* 2008), and biological materials appear to employ the same strategy. Figure 9 compares the strain energy of the gap between the sutured and unsutured bars. The viscoelastic gap material of the sutured bar allowed for energy dissipation since the strain energy in viscoelastic material is proportional to the damping (Plunkett 1992).

3.2. Design variables affecting to stress wave mitigation

A sinusoidal patterned interface caused a local complex stress redistribution, which led to wave attenuation and wave dispersion. In order to examine the influence variables regarding a sinusoidal pattern and boundary conditions, the seven variables shown in figure 3 were investigated using FE analysis. For each case, a pressure decay as stress waves propagated along the bar was observed. Also, compressive waves (S11), flexural waves (S22), and shear waves (S12) were plotted to evaluate the transformation of longitudinal stress into the shear stress and flexural stress. Longitudinal waves were recorded when pressure wave reached the end, and both of maximum flexural waves and maximum shear waves were recorded while pressure traveled the structure. Generally, as the longitudinal wave decreased, the flexural waves and shear waves increased. As one variable changed, the other six variables were fixed with the default value indicated in figure 3.

3.2.1. The effect of the suture waviness

Waviness is defined as the wave height divided by the wave period. Waviness was varied in six cases of 0.25, 0.5, 0.75, 1, 1.25, and 1.5, in which the waviness height was fixed and the waviness width was changed. As the pressure wave traversed the sutured bar from the loading region to the free end, the magnitude of the pressure decreased when a suture was introduced (figure 4). However, with a suture, there was minimal relationship between waviness and damping as shown in figure 10(a). Figure 10(b) showed that generated shear stresses incurred the largest value at a waviness ratio of 0.5 and the generated flexural wave incurred the largest value at a waviness ratio of 1. Hence, the greatest conversion from a longitudinal stress to a shear stress and flexural stress were waviness ratios of 0.5 and 1. We note here that the waviness ratio shown in figure 1 is 1 ± 0.32 for the woodpecker beak; 2.44 ± 0.67 for the bison skull; 0.99 ± 0.15 for the ammonoid shell; and 0.97 ± 0.23 for the turtle shell.

3.2.2. The effect of the R_{suture}

R_{suture} is defined as the suture height divided by the bar thickness. The R_{suture} was changed as 0, 0.10, 0.33, 0.67, and 0.83. The height of the suture was changed as 0, 1.5, 5, 10 and 12.5 mm while the bar thickness was fixed at 15 mm. As the R_{suture} increased, the pressure when the stress wave reached the end of the bar decreased as shown in figure 10(c). Figure 10(d) showed that a greater R_{suture} increased the flexural stress and shear stress, but the compressional stress decreased. With respect to different animals and the human skull, the 'bar thickness' would be far greater. However, we are only concerned with the suture height but needed to normalize it with respect to some absolute dimension to distinguish this feature from the waviness ratio.

3.2.3. The effect of the thickness of the gap

The gap thickness varies at different length scales for the different animals. As such, we varied the sutured bar's gap thickness: 1, 2, 4, and 6 mm. The thickness of the gap did not affect the amount of stress dissipation (figure 10(e)) and did not show a big difference when comparing the shear stresses and flexural stresses (figure 10(f)) although the 2 mm, 4 mm, 6 mm of the gap thickness induced slightly more dissipation than the 1 mm gap.

3.2.4. The effect of the material properties

For the sutures in animals, the material comprises mainly collagen, a structural protein that behaves like a viscoelastic material. However, the material on either side of the viscoelastic collagen varied from bone to keratin to other biological materials. Material properties of the waveguide (the bar material in our study) determines the sound speed as the equations (5) and (6).

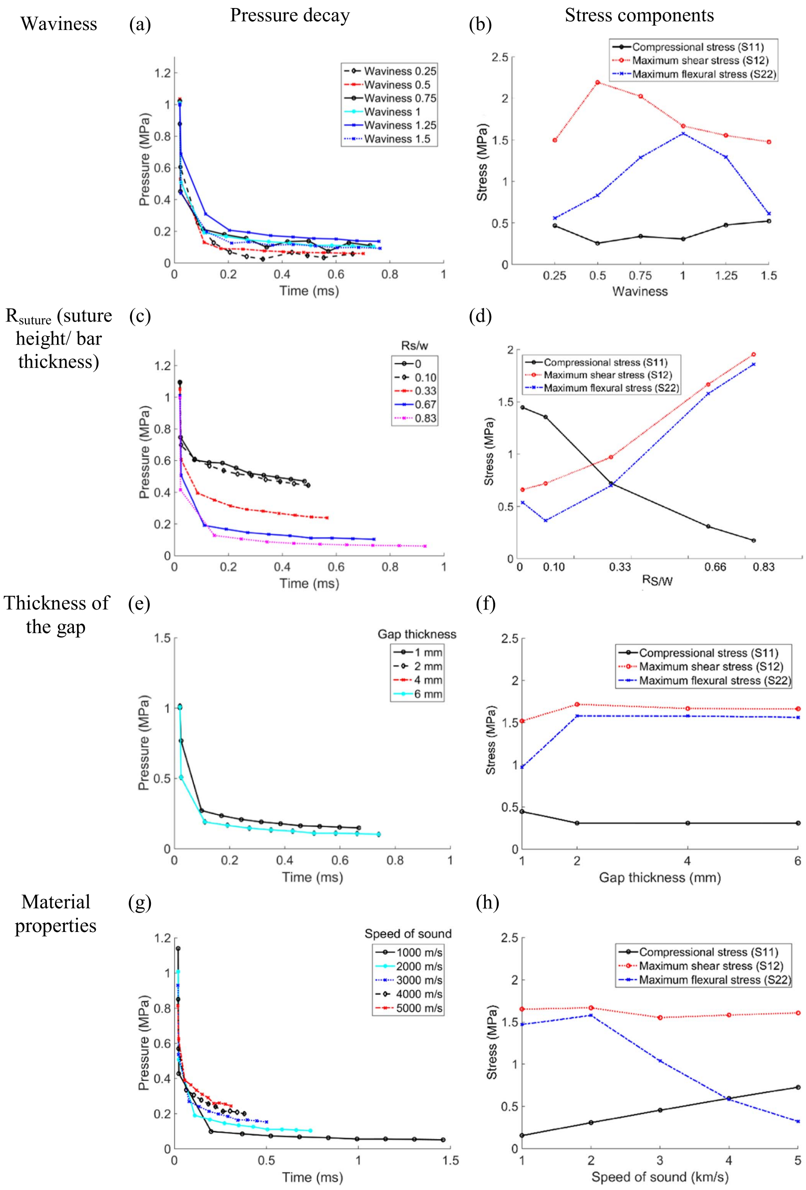

Figure 10. Pressure wave decay as pressure waves traveled from the load applied region to the free end at the idealized bar with a suture interface, and compressional stress when the stress wave reaches to the free end, maximum shear stress and maximum flexural stress while pressure wave traveling at seven variables of (a), (b) waviness, (c), (d) R_{suture} which is the ratio of the suture height to the bar thickness, (e), (f) thickness of the gap, (g), (h) material properties, (i)–(l) type of the wall boundary, (m), (n) amplitude of the loading, and (o), (p) impact duration. Each point in (k) is 10 mm apart while other points are 100 mm apart in the pressure decay graphs.

In this study, five different elastic moduli were simulated; 2, 8, 18, 32, and 50 GPa resulting in wave speeds of 1000, 2000, 3000, 4000, and 5000 m s^{-1} accordingly. The dissipation occurred greater as the wave speed decreased (figure 10(g)), and also the time arriving at the end of the bar decreased. Figure 10(h) shows that the generation of a shear wave was not affected by the wave speed while the generated flexural wave decreased as the wave speed increased. As the wave speed increased, the longitudinal compression stress proportionally increased when the stress wave reached the end of the bar.

3.2.5. Type of wall boundary

The effect of the boundary was illustrated by the in-phase, out-of-phase, only center, and only outside boundaries conditions (figures 10(i) and (j)). Stress wave dissipation was also examined with infinite boundaries of the side walls to remove the boundary effect (figures 10(k) and (l)). Figure 10(i) showed that there was no difference in the damping and wave speed between the in-phase and out-of-phase boundaries. However, when changing the suture boundary to a straight boundary increased the wave speed independent of the centerline suture geometry or outside boundary edge. Also, the results showed that an interaction exists between the suture and the gap for damping. Suture interfaces brought greater strain energy to the gap compared to flat interfaces as discussed in figure 8. Hence, the damping of the bar with an only-outside-suture in which the suture-gap interaction was absent was smaller than the other

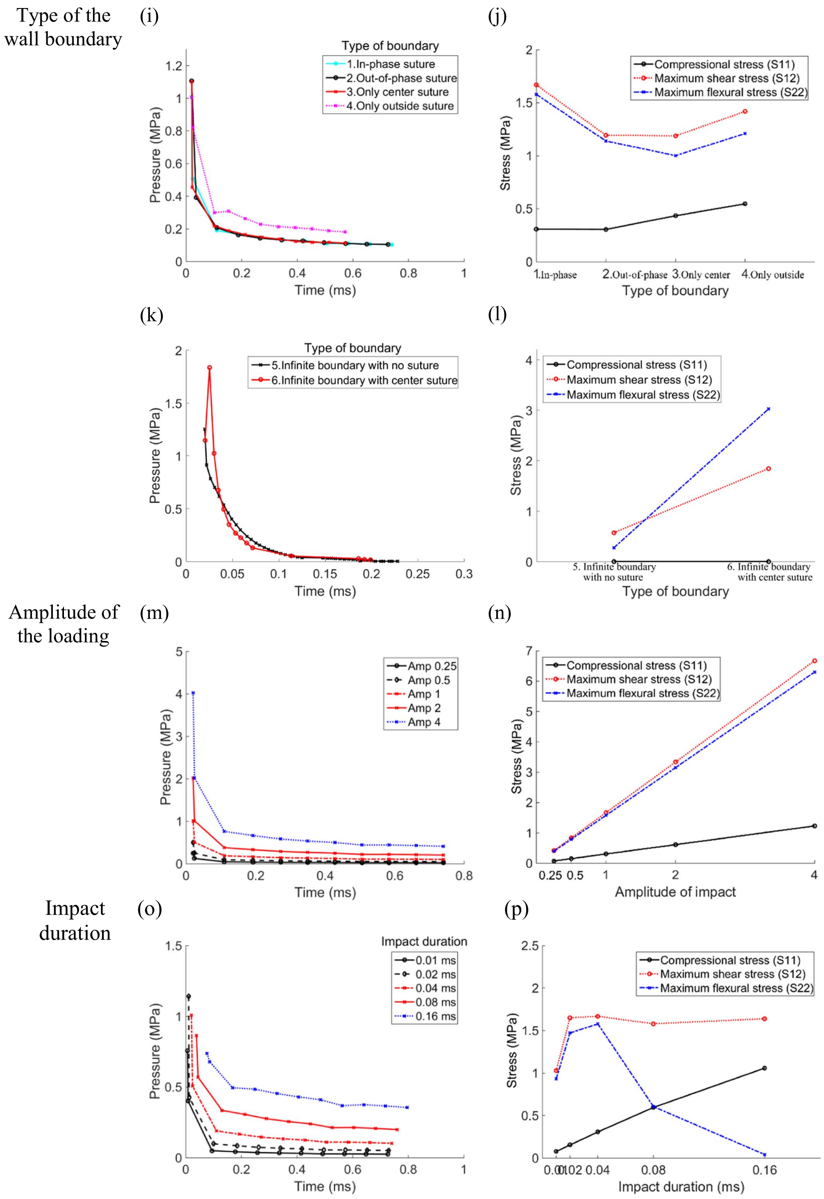

Figure 10. (Continued.)

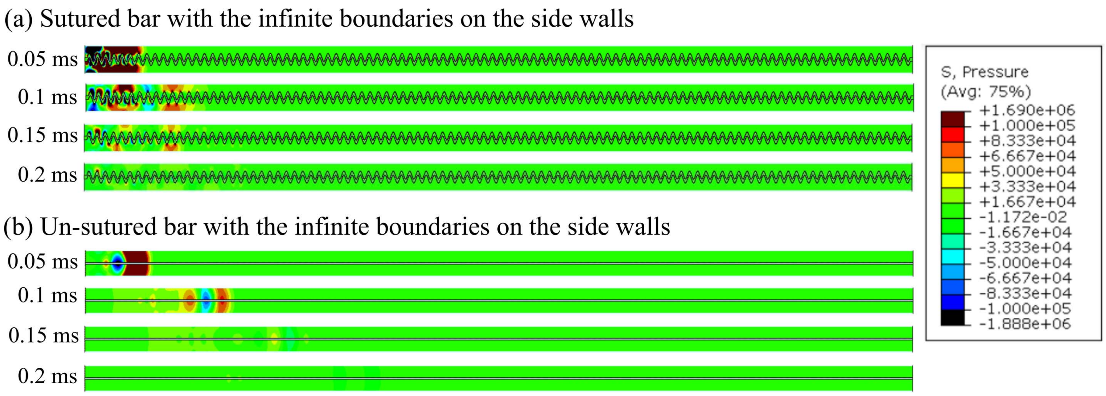

Figure 11. Pressure contour of (a) the sutured bar and (b) the unsutured bar with infinite boundaries on the side walls at the time of 0.15, 0.1, 0.15, and 0.2 ms. The pressure fully dissipated at 140 mm away from loading edge in the sutured bar and 460 mm away in the unsutured bar.

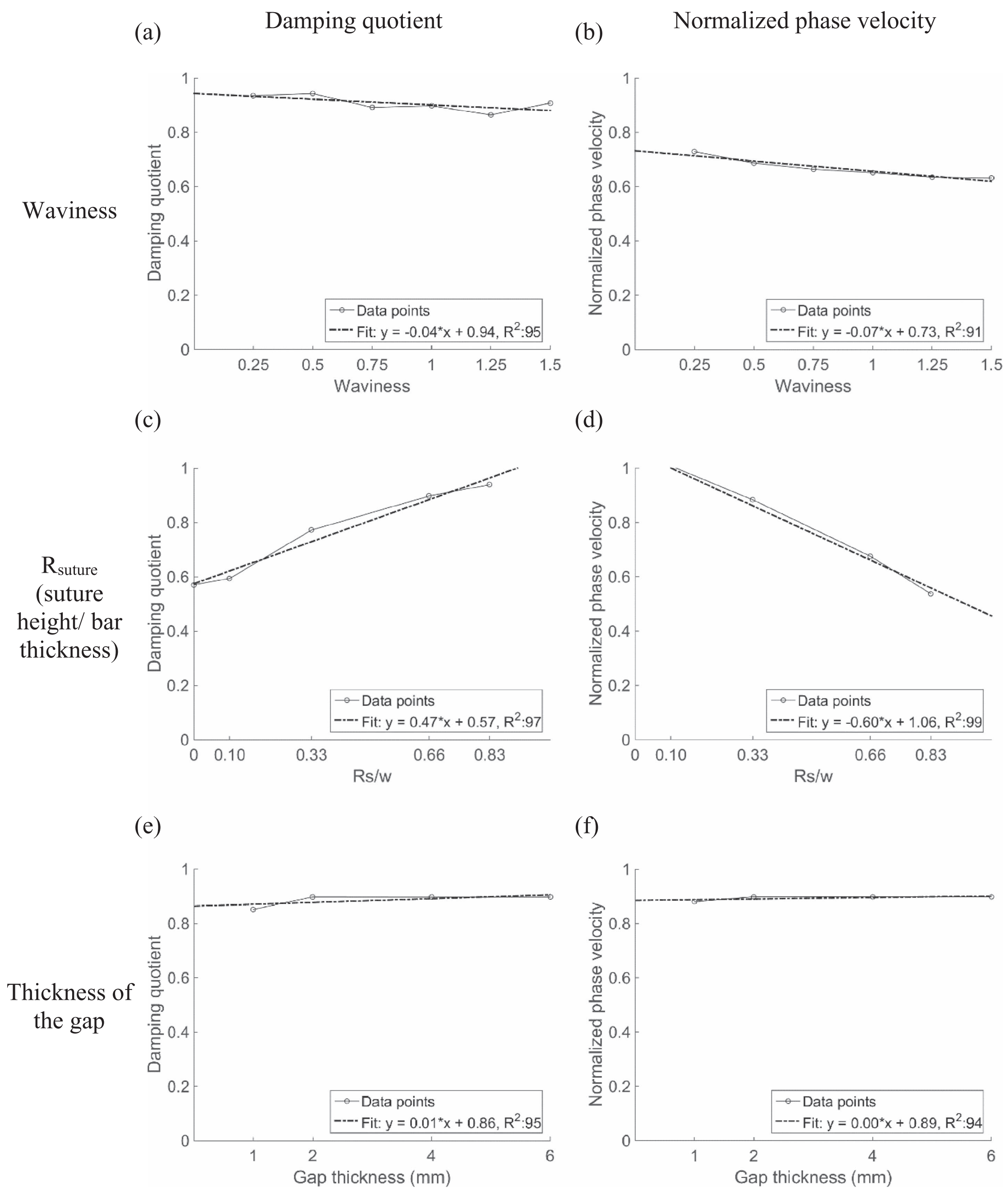

Figure 12. The data points of the damping quotient with its associated the curve fit and the data points of the normalized phase velocity and the curve fitting at seven variables of (a), (b) waviness, (c), (d) R_{suture} (ratio of the suture height to the bar thickness), (e), (f) thickness of the gap, (g), (h) material properties, (i)–(l) type of wall boundaries, (m), (n) loading amplitude, and (o), (p) impact duration.

configurations. Figure 10(j) showed the stress transformation at the four types of boundaries. Although the damping and wave speed were similar in in-phase and out-of-phase suture boundaries, the maximum shear stress and the maximum flexural stress were greater at the in-phase boundary than those of out-of-phase boundary.

Figure 10(k) shows the pressure decay for the bars with infinite boundaries on the side walls. Pressure was recorded every 10 mm not 100 mm, because the pressure dissipated quickly compared to the bars with finite boundaries. Figure 10(k) demonstrated that the suture slows down the stress wave and dissipates the wave quicker than the unsutured bar. For the sutured bar, the pressure increased from the edge up to 10 mm away from the loaded edge due to the reflected S11 waves and generated S22 waves. The pressure then decreased rapidly and dissipated fully after traveling 140 mm away from the loaded edge at 0.20 ms (figure 11(a)). On the other hand, for the unsutured bar, the stress wave completely dissipated after traveling 460 mm away from the loaded edge at 0.23 ms (figure 11(b)). The calculated wave speed was 700 m s^{-1} in the sutured bar and 2000 m s^{-1} in the unsutured bar. Figure 10(l) shows that both the generated maximum shear stress and maximum flexural stress during stress wave propagation

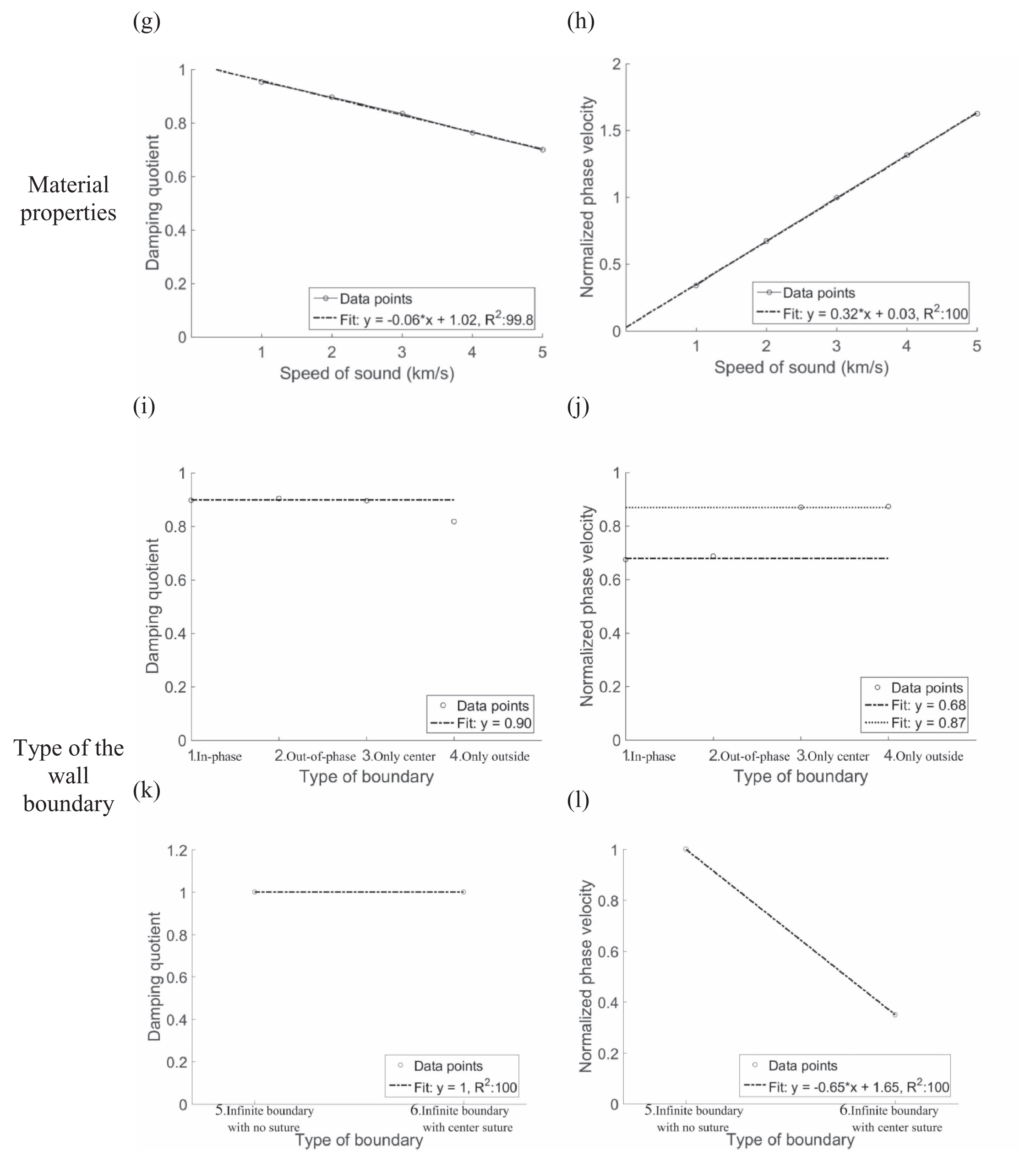

Figure 12. (Continued.)

were greater in the sutured bar than those in the unsutured bar. The maximum shear stress in the sutured bar (3.02 MPa) was approximately 11.2 times greater than that in the unsutured bar (0.27 MPa), and the maximum flexural stress in the sutured bar (1.84 MPa) was approximately 3.2 times greater than that in the unsutured bar (0.57 MPa).

3.2.6. The effect of the amplitude of the impulsive loading

The amplitude of the impact loading was changed as 0.25, 0.5, 1, 2, and 4 to investigate the damping effects caused by an input condition of amplitudes. As the amplitude of impact increased, the pressure also increased. However, the damping amounts remained the same regardless of the amplitude of the loading as shown in figure 10(m). Figure 10(n) showed that as the amplitude of the loading increased, the stresses S11, S12, and S22 also increased.

3.2.7. The effect of the impact duration

The impact duration of the loaded pressure wave was changed to 0.01, 0.02, 0.04, 0.08, and 0.16 ms in order to investigate the damping effects resulting by an input condition of different periods (and/or frequencies). Results showed that as the impact duration increased, less dissipation occurred regarding the pressure wave (figure 10(o)), and the compressional stress converted less to the flexural stress (figure 10(p)). Hence, we can

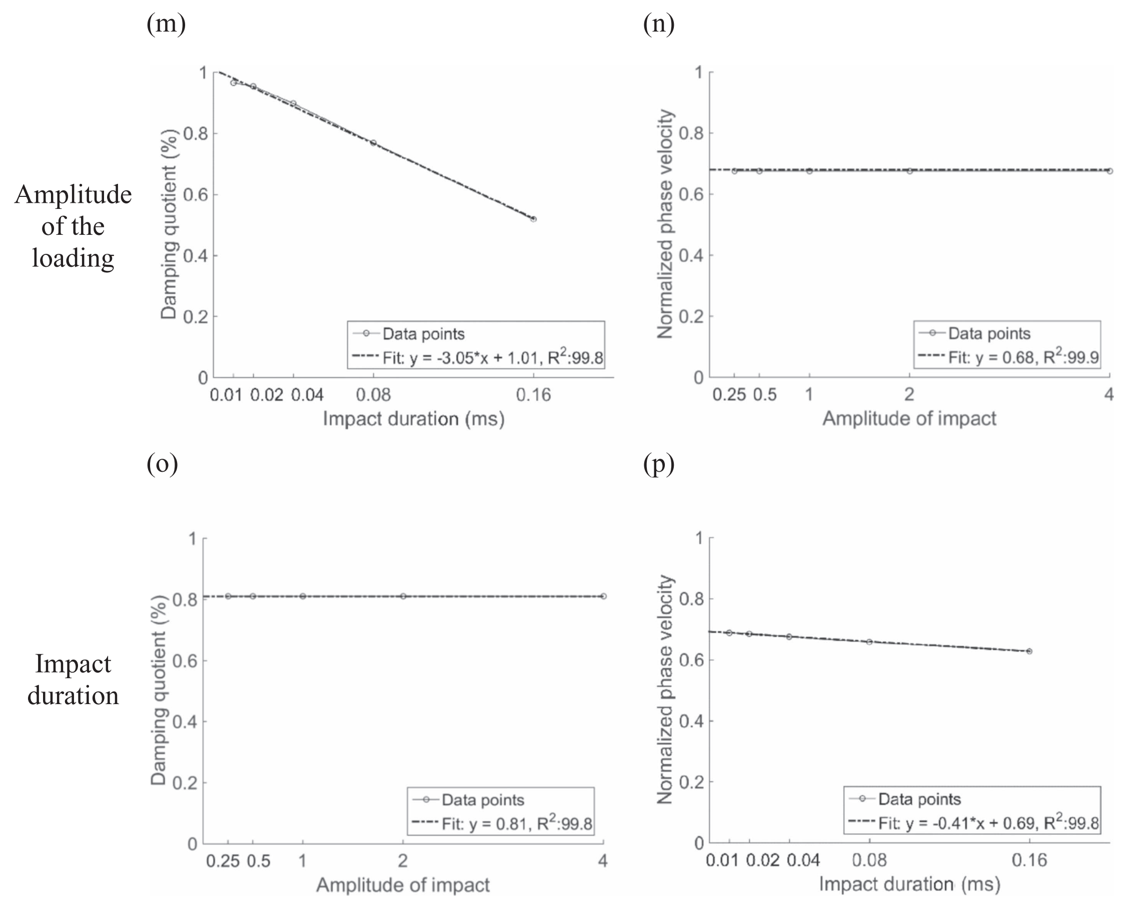

Figure 12. (Continued.)

conclude that as the impact becomes faster and faster, the effect of the suture gets greater and greater in terms of dissipating the stress wave!

3.3. Damping quotient and phase velocity

The damping quotient and normalized phase velocity were evaluated to quantify the variables' effects on stress wave mitigation. Figure 12 shows the correlation of each variable with respect to the attenuation and dispersion of the pressure waves.

Figures 12(a) and (b) show the relationships between waviness and the damping quotient/phase velocity. Because of the minimal relationship between the suture waviness and damping quotient as evinced by a slope value of 0.04 (R^2:45), and between the waviness and phase velocity with a slope value of 0.07 (R^2:91), the suture waviness essentially did not affect the damping. R_{suture} versus damping quotient was illustrated in figure 12(c) to show that the damping quotient was proportional to the R_{suture}. The damping quotient increased from 0.57 to 0.94 as the R_{suture} increased from 0 to 0.83. Hence, for every unit increment increase of R_{suture} gives a 45% increase of damping. Also, the normalized phase velocity proportionally decreased as R_{suture} increased (figure 12(d)). Jaslow (1990) reported that the amount of energy absorbed may depend on the morphology of the suture, and our findings indicated that the amount of energy mitigated was directly related to R_{suture} rather than the waviness. Figures 12(e) and (f) show that the gap thickness did not substantially affect the wave dissipation and dispersion. Figures 12(g) and (h) show that the sound speed determined by material properties gave changes in damping and phase velocity proportionally but less than the R_{suture} effect. Regarding the type of boundary with finite boundaries, there was no difference in the damping quotient and phase velocity between the in-phase and out-of-phase sutures while the absence of suture lines led to less attenuation and dispersion as shown in figures 12(i) and (j). For the bars with infinite boundaries, the damping quotients were unity in both the sutured and unsutured bars, because all the pressure waves were dissipated before reaching the end (figure 12(k)). However, sutures played an important role in dispersing the pressure waves in the bar with infinite boundaries (figure 12(l)) as the wave speed velocity was reduced 65%. Figures 12(m) and (n) show that the impact amplitude did not correlate to the damping quotient and phase velocity. Figures 12(o) and (p) indicate that the impact duration affected the wave attenuation but not the wave dispersion. As a result, the three variables including R_{suture}, speed of sound, and impact duration affected the damping quotient, and two variables including R_{suture}, speed of sound affected the normalized phase velocity.

4. Conclusions

One unique characteristic of biological materials is the effective use of elasticity and viscoelasticity for mitigating and dissipating energy. Although shock absorbers such as car bumpers or guard rails are designed to absorb impact energy through plastic deformation, biological materials cannot use this strategy for absorbing energy, because severe plastic deformation could cause fatal damage. To keep structural integrity, biological materials use elastic and viscoelastic responses effectively to dampen stress waves and absorb energy. Sutures are found in nature in which energy absorption and stress wave damping are important, and they function in two roles: (i) suture interfaces transform longitudinal waves into shear waves and flexural waves so that elastic deformation arises in not only the longitudinal direction but the transverse and shear directions as well; and (ii) the interaction between viscoelastic material in the gap and suture geometry lead to stress wave damping.

In addition, we investigated variations of suture interfaces and boundary conditions to evaluate their correlation to damping. As a result, there were three variables that increased wave attenuation: (i) high ratio of the suture height to the bar thickness, (ii) a short external impact duration, and (iii) low sound speed dictated by the elastic modulus. The two variables causing wave dispersion were a high ratio of the suture height over the bar thickness and a low sound speed. If the material properties and impact duration cannot be controlled in the engineering design of a structural component or system, making the suture height greater becomes the only controllable design variable that matters.

Acknowledgments

The authors would like to acknowledge the support from the Department of Agricultural and Biological Engineering, the Department of Mechanical Engineering, and the Center for Advanced Vehicular Systems (CAVS) at Mississippi State University. Effort sponsored by the Engineering Research & Development Center under Cooperative Agreement number W912HZ-15-2-0004. The views and conclusions contained herein are those of the authors and should not be interpreted as necessarily representing the official policies or endorsements, either expressed or implied, of the Engineering Research & Development Center or the US Government.

ORCID

Sungkwang Mun https://orcid.org/0000-0002-3347-2587

References

Allen E 2007 *Cephalopods Present and Past: New Insights and Fresh Perspectives* (Cham: Springer) pp 159–80

Allen E G 2006 New approaches to fourier analysis of ammonoid sutures and other complex, open curves *Paleobiology* **32** 299

Behrents R G, Carlson D S and Abdelnour T 1978 *In vivo* analysis of bone strain about the sagittal suture in Macaca mulatta during masticatory movements *J. Dental Res.* **57** 904–8

Berthelot J-M, Assarar M, Sefrani Y and El Mahi A 2008 Damping analysis of composite materials and structures *Compos. Struct.* **85** 189–204

Bosboom E, Hesselink M, Oomens C, Bouten C, Drost M and Baaijens F 2001 Passive transverse mechanical properties of skeletal muscle under *in vivo* compression *J. Biomech.* **34** 1365–8

Brekhovskikh L M and Goncharov V 2012 *Mechanics of Continua and Wave Dynamics* (Berlin: Springer)

Byron C D 2006 Role of the osteoclast in cranial suture waveform patterning *Anatomical Rec.* A **288A** 552–63

Chen I H, Yang W and Meyers M A 2015 Leatherback sea turtle shell: a tough and flexible biological design *Acta Biomater.* **28** 2–12

Cheng T and Gan R Z 2007 Mechanical properties of stapedial tendon in human middle ear *J. Biomech. Eng.* **129** 913–8

Cupiał P and Niziol J 1995 Vibration and damping analysis of a three-layered composite plate with a viscoelastic mid-layer *J. Sound Vib.* **183** 99–114

Curtis N, Jones M, Evans S, O'Higgins P and Fagan M 2013 Cranial sutures work collectively to distribute strain throughout the reptile skull *J. R. Soc. Interface* **10** 20130442

DasGupta A and Hagedorn P 2007 *Vibrations and Waves in Continuous Mechanical Systems* (New York: Wiley)

De Blasio F V 2008 The role of suture complexity in diminishing strain and stress in ammonoid phragmocones *Lethaia* **41** 15–24

Graff K F 1975 *Wave Motion in Elastic Solids* (New York: Dover)

Herring S W and Teng S 2000 Strain in the braincase and its sutures during function *Am. J. Phys. Anthropol.* **112** 575

Hubbard R P, Melvin J W and Barodawala I T 1971 Flexure of cranial sutures *J. Biomech.* **4** 491–2

Jaslow C R 1990 Mechanical propertise of cranial sutures *J. Biomech.* **23** 313–21

Krauss S, Monsonego Ornan E, Zelzer E, Fratzl P and Shahar R 2009 Mechanical function of a complex three-dimensional suture joining the bony elements in the shell of the red eared slider turtle *Adv. Mater.* **21** 407–12

Lee N, Horstemeyer M, Rhee H, Nabors B, Liao J and Williams L N 2014 Hierarchical multiscale structure–property relationships of the red-bellied woodpecker (*Melanerpes carolinus*) beak *J. R. Soc. Interface* **11** 20140274

Li B-W, Zhao H-P, Qin Q-H, Feng X-Q and Yu S-W 2012a Numerical study on the effects of hierarchical wavy interface morphology on fracture toughness *Comput. Mater. Sci.* **57** 14–22

Li Y, Ortiz C and Boyce M C 2011 Stiffness and strength of suture joints in nature *Phys. Rev.* E **84** 062904

Li Y, Ortiz C and Boyce M C 2012b Bioinspired, mechanical, deterministic fractal model for hierarchical suture joints. *Phys. Rev.* E **85** 031901

Li Y, Ortiz C and Boyce M C 2013 A generalized mechanical model for suture interfaces of arbitrary geometry *J. Mech. Phys. Solids* **61** 1144–67

Lin E, Li Y, Ortiz C and Boyce M C 2014a 3D printed, bio-inspired prototypes and analytical models for structured suture interfaces with geometrically-tuned deformation and failure behavior *J. Mech. Phys. Solids* **73** 166–82

Lin E, Li Y, Weaver J C, Ortiz C and Boyce M C 2014b Tunability and enhancement of mechanical behavior with additively manufactured bio-inspired hierarchical suture interfaces *J. Mater. Res.* **29** 1867–75

Maloul A, Fialkov J, Wagner D and Whyne C M 2014 Characterization of craniofacial sutures using the finite element method *J. Biomech.* **47** 245–52

Opperman L A 2000 Cranial sutures as intramembranous bone growth sites *Develop. Dyn.* **219** 472–85

Plunkett R 1992 *Damping Analysis: An Historical Perspective* (West Conshohocken, PA: ASTM) pp 562–9

Saravanos D and Pereira J 1992 Effects of interply damping layers on the dynamic characteristics ofcomposite plates *AIAA J.* **30** 2906–13

Seimetz C N, Kemper A R and Duma S M 2012 An investigation of cranial motion through a review of biomechanically based skull deformation literature *Int. J. Osteopathic Med.* **15** 152–65

Sun Z, Lee E and Herring S W 2004 Cranial sutures and bones: growth and fusion in relation to masticatory strain *Anatomical Rec.* A **276** 150–61

Ubukata T, Tanabe K, Shigeta Y, Maeda H and Mapes R H 2010 Eigenshape analysis of ammonoid sutures *Lethaia* **43** 266–77

Yu J C, Borke J L and Zhang G 2004 Brief synopsis of cranial sutures: optimization by adaptation *Semin. Pediatric Neurol.* **11** 249–55

Zhang Z and Yang J 2015 Biomechanical dynamics of cranial sutures during simulated impulsive loading *Appl. Bionics Biomech.* **2015**